Energy and Momentum Transfer in Air Shocks

John W. Hutchinson
School of Engineering and Applied Sciences,
Harvard University,
Cambridge, MA 02138

A series of one-dimensional studies is presented to reveal basic aspects of momentum and energy transfer to plates in air blasts. Intense air waves are initiated as either an isolated propagating wave or by the sudden release of a highly compressed air layer. Wave momentum is determined in terms of the energy characterizing the compressed layer. The interaction of intense waves with freestanding plates is computed with emphasis on the momentum and/or energy transferred to the plate. A simple conjecture, backed by numerical simulations, is put forward related to the momentum transmitted to massive plates. The role of the standoff distance between the compressed air layer and the plate is elucidated. Throughout, dimensionless parameters are selected to highlight the most important groups of parameters and to reduce parametric dependencies to the extent possible. [DOI: 10.1115/1.3129773]

1 Introduction

Numerical analysis codes such as LS-DYNA, DYSMAS, and ABAQUS have been used for some time to model specific fluid-structure interactions (FSI) involving structures subject to blast loads generated in water and air environments. These powerful tools permit engineers to pose and solve complicated practical problems. In part, because of the availability of these codes, there has been little inclination in recent years to investigate some of the most elementary aspects of fluid-structure interaction relevant to structural design. Fundamental understanding of the role of intense blast loads on structures in water, which provided the momentum transferred to a plate struck by a planar wave, is grounded in results obtained years ago, such as those of Taylor [1] and Cole [2]. Recently, a significant advancement in basic knowledge became available through an extension of these results to intense air shocks by Kambouchev et al. [3,4], which will subsequently be referred to as the KNR theory. The study of basic one-dimensional fluid-structure interaction problems for air blasts is continued in this paper to elucidate behavior and to add to the store of relatively simple fundamental results.

Section 2 introduces some of the properties of intense planar waves. A standard device for bypassing detailed modeling of an explosive charge employing the sudden release of a highly compressed layer is introduced, and the connection between the source energy and wave momentum is established. The results of Taylor for a plate struck by an isolated planar wave are reviewed briefly in Sec. 3 with additional results for fluid-structure interactions in air supplementing those of KNR. The role of proximity of the compressed layer to the plate is studied in Sec. 4. The results for energy and momentum transfer to the plate are given as a function of the standoff distance between the plate and the compressed layer.

2 Isolated One-Dimensional Blast Waves

2.1 Linear Compression Waves in Water. Nonlinear compressibility effects of blast waves propagating in water are relatively small unless the peak pressures are in excess of 100 MPa, but they do give rise to a shocklike front and followed by exponentially decaying intensity. Valuable fluid-structure interaction results for water blast waves can be obtained using linear wave mechanics with cavitation modeled when the pressure in the water becomes negative. The result of Taylor [1] and Cole [2] for momentum transfer to a plate struck by a blast wave is such an example. An isolated planar wave propagating in the positive x-direction through water is modeled as being exponential in form with particle velocity $v=v_0 f(\xi)$ and overpressure $\Delta p=\Delta p_0 f(\xi)$, where $\xi=x-ct$ and

$$f(\xi)=0, \quad \xi>0$$
$$f(\xi)=e^{\xi/\ell}, \quad \xi<0 \tag{1}$$

The peak overpressure and particle velocity are related by $\Delta p_0=\rho c v_0$ with ρ as the ground state density, $c=\sqrt{B/\rho}$ as the wave speed, and B as the compressibility modulus. The decay time associated with the exponential shape is $t_0=c/\ell$. Generally, the ambient pressure in the water is very small compared with Δp_0, and it is neglected in the Taylor analysis. In this case, the total wave energy/area ΔE_0 is equally partitioned between the energy associated with the overpressure $\int \Delta p^2/(2B)dx$ and the kinetic energy $\int \rho v^2/2dx$ for isolated planar waves of any shape $f(\xi)$. The momentum/area is $I_0=\int \rho v dx$. For the exponential wave, these are

$$I_0=\Delta p_0 t_0=\rho v_0 \ell, \quad \Delta E_0=(\Delta p_0^2 \ell/B)/2=\rho v_0^2 \ell/2 \tag{2}$$

2.2 Nonlinear Compression Waves in Air. The nonlinear compressibility of air plays an essential role in the evolving shape changes experienced by intense planar waves. An intense wave propagating into quiescent ambient air develops a shock front with a shape that evolves as the wave advances. Because the wave speed increases with pressure due to nonlinear compressibility, the front of the wave propagates faster than rear portions of the wave such that as the wave propagates its width increases and its peak pressure decreases. Here, selected analytic results from the nonlinear theory of one-dimensional planar waves propagating in air [5] will be used along with numerical methods [6,7,3] to establish the results, which follow in the paper. Throughout, air is treated as an ideal gas with gas constant R and $\gamma=1.4$ as the ratio of the specific heats. Artificial viscosity will be introduced in the numerical simulations.

Let p_{atm}, ρ_{atm}, and $c_{\text{atm}}=\sqrt{\gamma p_{\text{atm}}/\rho_{\text{atm}}}$ be the pressure, density, and wave speed in air under ambient atmospheric conditions, respectively. Consider adiabatic propagation of a rightward moving isolated planar wave with smooth velocity $v=f(x)$ at $t=0$. For $t>0$, prior to shock formation, the distributions of the velocity, pressure, density and wave speed are governed by the following nonlinear implicit equations [5]:

$$v=f(x-(c+v)t)$$

Contributed by the Applied Mechanics Division of ASME for publication in the JOURNAL OF APPLIED MECHANICS. Manuscript received July 28, 2008; final manuscript received January 27, 2009; published online June 15, 2009. Review conducted by Ashkan Vaziri.

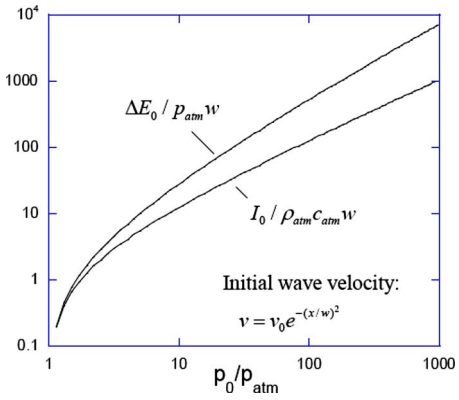

Fig. 1 Normalized wave energy/area and momentum/area for a isolated right-ward moving planar wave with an initial peak pressure p_0 in air and a prescribed velocity distribution

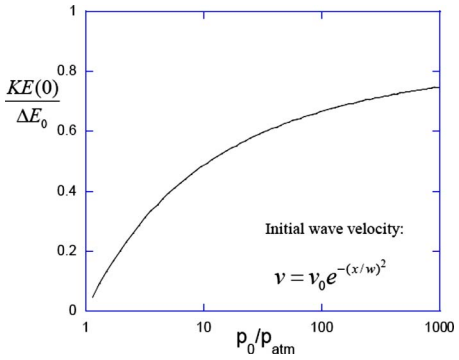

Fig. 2 Ratio of kinetic energy/area at $t=0$ to total wave energy/area as a function of initial peak pressure for a wave with a prescribed initial velocity distribution

$$\frac{p}{p_{\text{atm}}} = \left(\frac{\rho}{\rho_{\text{atm}}}\right)^{\gamma} = \left(\frac{c}{c_{\text{atm}}}\right)^{2\gamma/(\gamma-1)} = \left[1 + \frac{\gamma-1}{2}\frac{v}{c_{\text{atm}}}\right]^{2\gamma/(\gamma-1)} \tag{3}$$

This result will be used as an initial condition to initiate rightward moving waves with specified momentum and in some of the numerical simulations.

These results can also be used to establish the momentum and total wave energy for specific waves and the kinetic and internal energies at a given instant of time prior to shock formation. The momentum/area of the wave I_0 is independent of time as follows:

$$I_0 = \rho_{\text{atm}} c_{\text{atm}} \int_{-\infty}^{\infty} \left(\frac{\rho}{\rho_{\text{atm}}}\frac{v}{c_{\text{atm}}}\right) dx \tag{4}$$

The kinetic energy/area varies with time such that

$$\text{KE}(t) = \frac{1}{2}\gamma p_{\text{atm}} \int_{-\infty}^{\infty} \frac{\rho}{\rho_{\text{atm}}}\left(\frac{v}{c_{\text{atm}}}\right)^2 dx \tag{5}$$

The total wave energy/area is also independent of time; it is the sum of the kinetic energy and excess internal energy (the internal energy minus the ambient energy).

$$\Delta E_0 = \text{KE}(t) + \frac{p_{\text{atm}}}{\gamma-1}\int_{-\infty}^{\infty}\left[\frac{p}{p_{\text{atm}}} - \left(\frac{p}{p_{\text{atm}}}\right)^{1/\gamma}\right] dx \tag{6}$$

which is only valid prior to shock formation and with no dissipation. For example, for a wave with the velocity distribution at $t=0$,

$$v = v_0 e^{-(x/w)^2} \tag{7}$$

numerical integration provides the plots of momentum and total wave energy as a function of p_0/p_{atm} in Fig. 1, where p_0 is the maximum pressure at $t=0$ related to v_0 by Eq. (3). The ratio of the kinetic energy to total wave energy at $t=0$ is plotted as a function of p_0/p_{atm} in Fig. 2. The more intense the wave, the larger is the kinetic energy as a fraction of the total wave energy. These results depend on the details of the velocity distribution, but the trends expressed in term of peak pressure are representative. In Fig. 2, $\text{KE}(0)/\Delta E_0$ does not approach $\frac{1}{2}$ for low intensity waves, as seen for water blasts, because the ambient air pressure cannot be neglected for low intensity air waves.

The numerical method employed to analyze the series of one-dimensional problems presented below is based on the widely used von Neumann–Richtmyer algorithm [6], which incorporates artificial viscosity in the model of the gas to smoothen the shock discontinuities and to stabilize the solution procedure. The viscous contributions are added in a manner, which preserves energy conservation. The present formulation follows that are used in the KNR studies [3] and are detailed in the text [7]. The equations governing the constitutive behavior of the air are as follows. Let p, ρ, and T be the pressure, mass density, and temperature in the current state, respectively. The internal energy/mass is given by $e=RT/(\gamma-1)$. Denote the normal stress contribution due to viscosity by Q such that the ideal gas law is modified as

$$p = \rho RT - Q \tag{8}$$

Following Refs. [3,7], the artificial viscosity contribution is taken as $Q=0$ for $\dot{\varepsilon} > 0$ and

$$Q = -\rho_i[(b_1\dot{\varepsilon}\Delta)^2 + b_2 c|\dot{\varepsilon}|\Delta], \quad \dot{\varepsilon} < 0 \tag{9}$$

where $\dot{\varepsilon}$ is the strain-rate, ρ_i is the initial density, Δ is a measure of the smeared shock thickness related to the current mesh size, $c = \sqrt{\gamma(\gamma-1)e}$ is the current sound speed, and b_1 and b_2 are the dimensionless viscosity coefficients. The time rate of the internal energy is taken to be consistent with energy conservation ($-p\dot{\varepsilon} = \rho\dot{e}$) as

$$\dot{e} = \left[-(\gamma-1)e + \frac{Q}{\rho}\right]\dot{\varepsilon} \tag{10}$$

The regions on the x-axis occupied by the air at $t=0$ are divided into a uniform mesh. The plate is represented as a freestanding plane with mass/area m_p. The description is Lagrangian with the positions of the material points as independent variables. The equations for the nonlinear behavior of an ideal gas are discretized in a manner that conserves momentum and energy. The results presented in the paper have been computed with between 2000 and 5000 mesh points, depending on the problem, with time steps set in accord with the stability requirements of the algorithm [3,7]. The viscosity coefficients were set at $b_1=2$ and $b_2=1$.

2.3 Waves Generated by a Sudden Release of Highly Pressurized Air. In numerical simulations, a useful device to simulate blast waves is to suddenly release a "container" of adiabatically compressed air that is initially at rest and that then pushes into quiescent ambient air. To this aim, consider a one-dimensional layer of air under ambient conditions of width h_{atm}, which is compressed adiabatically with no dissipation to thickness h. The excess energy/area in air in the compressed layer ΔE_0, excluding the energy of the air in its ambient state, is

$$\Delta E_0 = \frac{1}{\gamma-1}[p_0 h - p_{\text{atm}} h_{\text{atm}}] = \frac{p_{\text{atm}} h}{\gamma-1}\left[\frac{p_0}{p_{\text{atm}}} - \left(\frac{p_0}{p_{\text{atm}}}\right)^{1/\gamma}\right] \tag{11}$$

with $p_0/p_{\text{atm}} = (h_{\text{atm}}/h)^{\gamma}$. For example, a layer with $h_{\text{atm}}=0.27$ m that is squeezed to $h=0.01$ m produces $p_0/p_{\text{atm}}=100$ and $\Delta E_0 = 0.19$ MJ/m^2.

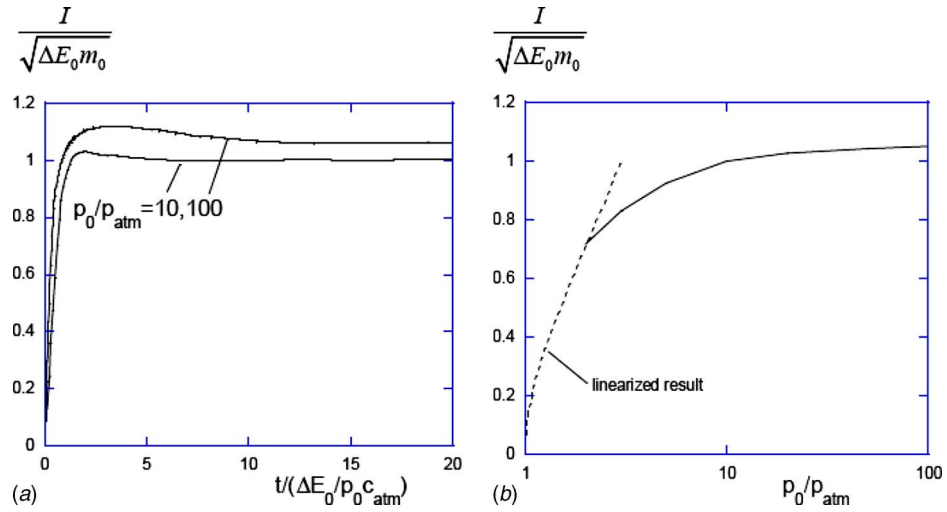

Fig. 3 Normalized momentum/area of rightward traveling wave produced by an initially compressed air layer with excess energy/area ΔE_0, mass/area m_0, and pressure p_0. (*a*) Momentum/area versus time for two initial pressures. (*b*) Momentum/area of the emerged wave.

Let $I(t)$ be the momentum/area of the rightward moving wave generated by the sudden release of the compressed air at $t=0$. The result will apply to a compressed layer of thickness h and excess energy/area ΔE_0 bounded by quiescent ambient air on its right and a rigid wall on the left or, equally, by symmetry, to a symmetrically placed compressed layer of thickness $2h$ and excess energy/area $2\Delta E_0$ bounded by quiescent air on both sides. As the wave propagates to the right, a shocklike front forms whose steepness is controlled by the artificial viscosity. The shape of the wave slowly evolves as described earlier. At any instant the wave energy is

$$\Delta E = \int \left[\frac{1}{2}\rho v^2 + \rho(e - e_{\text{atm}}) \right] dx \tag{12}$$

with integration in the current state for $0 \le x < \infty$ and $e_{\text{atm}} = p_{\text{atm}}/[(\gamma-1)\rho_{\text{atm}}]$. The wave energy is constant with $\Delta E = \Delta E_0$ given by Eq. (11), a feature that is preserved by the numerical scheme.

With $x=0$ at the edge of the rigid wall (or at the symmetry plane), $I = \int_0^\infty \rho v\, dx$ is the momentum/area of all the air occupying $x \ge 0$. By dimensional analysis, one can show that the entire parametric dependence for air modeled as an ideal gas is captured by the dimensionless form

$$\frac{I}{\sqrt{\Delta E_0 m_0}} = F\left(\frac{p_0}{p_{\text{atm}}}, \frac{t}{\Delta E_0/(p_0 c_{\text{atm}})} \right) \tag{13}$$

with a dependence on both γ and the viscosity coefficients being implicit. Here, $m_0 = \rho_0 h = \rho_{\text{atm}} h_{\text{atm}}$ is the mass/area of the compressed air layer. Initially at $t=0$ when the compressed layer is released, $I=0$, but in a very short period of time $(t/[\Delta E_0/(p_0 c_{\text{atm}})] \approx 1)$ an isolated compression wave forms and propagates to the right. Thereafter, I is nearly constant as can be seen in Fig. 3(*a*). The momentum in the air occupying $x \ge 0$ is not strictly constant because of interaction with the wall. After reaching a maximum, I decreases slightly as the pressure at the wall drops below p_{atm} and, subsequently, I increases slightly when the wall pressure rises again above p_{atm}. However, to a very good approximation, I is constant once an isolated wave emerges, and the normalized momentum of the wave $I/\sqrt{\Delta E_0 m_0}$ depends essentially only on p_0/p_{atm}. This dependence is plotted in Fig. 3(*b*) with I evaluated at its minimum value following the first maximum. The success of the particular normalization is evident in that $I/\sqrt{\Delta E_0 m_0} \approx 1$ for intense "explosions." Included in this figure is the result obtained by a linearized analysis in which p_0/p_{atm} is perturbed about unity as follows:

$$\frac{I}{\sqrt{\Delta E_0 m_0}} = \sqrt{\frac{1}{2}\left(\frac{p_0}{p_{\text{atm}}} - 1 \right)} \tag{14}$$

These results are not new, although the normalization given above seems to be particularly useful for the present objectives. The power of dimensional analysis to reduce the parametric dependencies is laid out in texts such as Ref. [8], and related results have been presented in various sources including Refs. [9,10].

3 Interaction Between Intense Isolated Waves and a Freestanding Plate

Kambouchev et al. [3] extended Taylor's linear theory of fluid-structure interaction in water to intense planar air blasts. Formulas for the momentum transfer to a freestanding plate were developed and calibrated by accurate numerical simulations. These authors generated a rightward moving wave by releasing a highly compressed layer well to the left of the plate. The wave propagates, forms a shock, and evolves in shape before striking the plate. The authors fit an exponential pressure distribution to the wave $p = p_0 e^{-t/t_0}$ with peak pressure p_0 and decay time t_0, in the period of time when the wave passes the plate (simulated with the plate removed). The interaction of the wave with the plate is computed with emphasis on the maximum momentum/area I transmitted to the plate as a function of the wave characteristics at the instant the plate is impacted.

Here, the KNR approach is modified in several ways. (1) The initial condition is taken as a rightward moving isolated wave (3) with precisely defined momentum/area I_0 and wave energy/area ΔE_0. (2) The momentum/area transmitted to the plate I is normalized by the incident momentum I_0 and it is conjectured based on numerical simulations that the limit for a massive plate is $I = 2I_0$ for all incident blast waves. (3) The results are presented in dimensionless form using invariant measures I_0 and ΔE_0 of the wave intensity. (4) The plate interacts with ambient air on the side opposite the blast, which KNR neglects.

3.1 Wave Impinging on a Massive Plate. For massive plates $(m_p \to \infty)$, many computations have been performed for different initial wave shapes (3) launched at a wide range of distances from the plate for initial pressure peaks p_0 ranging from several times p_{atm} to $1000 p_{\text{atm}}$. In all cases, it has been found that to within a

few tenths of a percent the momentum/area transferred to the plate, or equivalently, the impulse/area acting on the plate is $I=2I_0$ with I_0 as the momentum/area of the incident wave (4). Concomitantly, within the same precision the momentum/area of the reflected wave is $-I_0$. As is well known, linear theory (e.g., Taylor's theory) gives precisely $I=2I_0$ for the limit of massive plates. Based on the above findings, it seems reasonable to conjecture that $I=2I_0$ holds for compressible air waves as well. The very small difference between the numerical results determined here and $I=2I_0$ is likely due to errors associated with the numerical method, but this has not been established.

To our knowledge there is no proof of this result for nonlinear compressible waves, nor does it appear to have been remarked upon in the literature. The fact that the reflected wave has momentum/area $-I_0$ is obviously consistent with equal and opposite propagating waves colliding subject to conservation of momentum and energy. By symmetry, this problem is the same as the wave impacting a massive plate. Moreover, the simple result $I=2I_0$ would be expected from a statistical mechanical model of an ideal gas with molecules represented as hard spheres that undergo perfectly elastic collisions. The constitutive equations of the continuum model of an ideal gas are derived from such a model. Nevertheless, it is not obvious that the solution to the full set of continuum equations governing the ideal gas preserves this simple result, especially with inclusion of artificial viscosity.

3.2 Wave Impinging Upon a Plate of Finite Mass/Area m_p. A rightward propagating wave prescribed by Eq. (7) is launched at $t=0$ in the direction of a plate whose surface directed toward the blast is initially located at $x=d$, with d/w sufficiently large such that there is no interaction between the plate and the wave at $t=0$. Ambient air exists on both sides of the plate. The region of the x-axis is taken to be sufficiently large such that no reflected waves impact the plate from either the left or the right. The plate accelerates upon impact of the blast wave, attaining a maximum velocity, and then begins a slow deceleration due to the fall-off in pressure on the blast side and the buildup of pressure on the back side of the plate as it plows into the air on that side. The objective is to determine the maximum momentum/area I transmitted to the plate as related to the incident momentum I_0.

One set of independent parameters determining I are m_p, v_0, w, d, p_{atm}, and ρ_{atm}, along with γ and the viscosity coefficients, which will be regarded as fixed. While $c_{\text{atm}}=\sqrt{\gamma p_{\text{atm}}/\rho_{\text{atm}}}$ is not independent, it can be used when convenient. The momentum/area I_0 and wave energy/area ΔE_0 of the incident wave defined in Eqs. (4) and (6) can be used in place of v_0 and w. These variables have the advantage that they are invariant measures of the incident wave intensity in the sense that they remain constant as the wave propagates and, moreover, they are less tied to the specificity of the initial launching conditions. Based on the set of independent variables—m_p, I_0, ΔE_0, d, p_{atm} and ρ_{atm}—it follows from dimensional analysis that the general functional dependence of the maximum momentum/area imparted to the plate I depends on three dimensionless parameters as

$$\frac{I}{I_0}=F\left(\beta,\frac{\Delta E_0}{c_{\text{atm}}I_0},\frac{p_{\text{atm}}d}{c_{\text{atm}}I_0}\right) \tag{15}$$

with

$$\beta=\frac{1}{2}\frac{I_0^2}{\Delta E_0 m_p} \tag{16}$$

The parameter β has been defined in terms of the wave invariants such that it coincides with Taylor's [1] fluid-structure interaction parameter for linear exponential waves (1) using the expressions in Eq. (2), i.e., $\beta=\rho\ell/m_p$ or, equivalently, $\beta=t_0/t_p$ with $t_p\equiv m_p/(\rho c)$. Taylor's result for the maximum momentum imparted to the plate in a water blast is

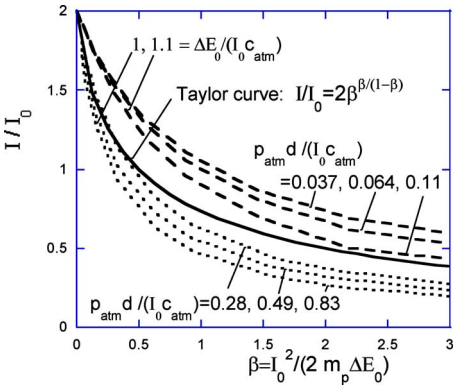

Fig. 4 Ratio of momentum/area transmitted to a plate to the momentum/area of the incident wave in terms of the generalized Taylor FSI parameter β in Eq. (16) and the two dimensionless parameters characterizing the wave. The values $\Delta E_0/I_0c_{\text{atm}}=1$ and 1.1 correspond to a wave (7) released with $w=0.05$ m with $p_0/p_{\text{atm}}=16$ and 127, respectively, at three distances from the plate ($d=0.4$ m, 0.7 m and 1.2 m.

$$\frac{I}{I_0}=2\beta^{\beta/(1-\beta)} \tag{17}$$

which is included in Fig. 4. In Taylor's water blast model, there is no restraint of water or air on the back side of the plate. The maximum momentum of the plate is attained when the pressure on the front side of the plate becomes negative, interpreted as the onset of cavitation.

Plots of I/I_0 as a function of the generalized β are presented in Fig. 4 for a range of initial conditions specified by the other two dimensionless parameters. An illustration in dimensional terms is included in the figure caption. It is seen that the fraction of the incident wave momentum transferred to the plate is primarily dependent on β with importance dependence on the other two parameters as well. Relatively small changes in $\Delta E_0/(c_{\text{atm}}I_0)$ are associated with large changes in p_0/p_{atm}. In spite of the differences in modeling, the trends in Fig. 4 are similar to the more extensive results presented by KNR [3], who used other measures of the incident wave intensity evaluated at the moment of impact and who also developed formulas that accurately reproduce their numerical results. Specifically, KNR generalized the Taylor parameter to intensify air blasts according to $\beta=t_0/t_p^*$ where $t_p^*\equiv m_p/(\rho_s U_s)$ with ρ_s as the density directly behind the shock front and U_s as the velocity of the shock front, both measured at the instant just before the wave hits the plate.

Figure 4 provides a unified way to view fluid-structure interaction between blast waves in water and air and a freestanding plate. Substantial reductions in momentum transfer due to fluid-structure interaction will only be achieved if $I_0^2/\Delta E_0$ is comparable to m_p. For relatively thick metallic plates, this will only occur for very intense air blasts. In air blasts, most plates acquire the maximum possible momentum/area $2I_0$.

An advantage of using β as defined in Eq. (16) to describe the fluid-structure interaction behavior is that this dimensionless variable is defined using invariants of the incident wave, whereas, for example, the choice $\beta=t_0/t_p^*$ favored by KNR must be determined in some manner (computation or test measurements) at the instant the wave strikes the plate. For a wave launched with specific momentum/area and excess energy/area, $\beta=t_0/t_p^*$ depends on the distance the wave travels to reach the plate. Conversely, a disadvantage of the present choice of β in Eq. (16), as opposed to that of KNR, is that the present choice does not reflect the fact that the intensity of the traveling wave diminishes with distance traveled. This deficiency is due to the fact that the wave energy ΔE_0 defined initially by Eq. (6) and subsequently by Eq. (12), includes internal

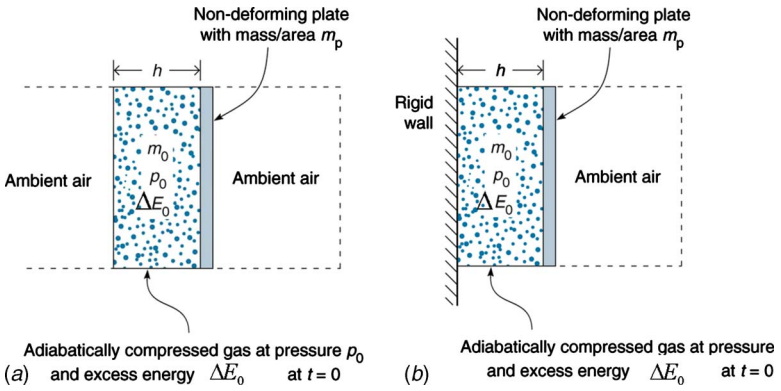

Fig. 5 Configuration and notation for simulations releasing compressed air layer at $t=0$ with no standoff distance to plate. (*a*) No backing to compressed layer. (*b*) Rigid backing to compressed layer.

energy (heat) in the "quiescent" air left behind the propagating wave. In the computational model, the remnant internal energy is set by the viscosity coefficients. In the absence of viscosity, the remnant energy is set by jump conditions across the shock. Thus, while the wave energy ΔE_0 is conserved, it does not faithfully measure the intensity available to accelerate the plate after the wave has traveled distances sufficient to leave behind an appreciable fraction of its initial energy as heat. These trends are made explicit in Fig. 4 through the dependence on $p_{\text{atm}}d/(c_{\text{atm}}I_0)$.

In conclusion, it has been noted that there are several ways to generalize Taylor's fluid-structure interaction parameter β for intense air blasts. The choice identified by KNR has the distinct advantage that it provides a measure of the relevant wave intensity at the instant the wave strikes the plate. As a consequence, it appears to reduce the dependence of I/I_0 on only one dimensionless parameter in addition to β, assuming wave has propagated far enough to have evolved into an exponential shape.

4 Energy and Momentum Imparted to a Plate by a Highly Compressed Layer of Air

4.1 The Role of Backing to the Compressed Air Layer for Plates With Zero Standoff. Consider the initial configurations in Fig. 5 wherein an adiabatically compressed air layer such as that introduced in Sec. 2.3 is released at $t=0$ and accelerates a plate in direct contact with the layer to the right. Two cases are considered: (a) no backing on the left of the layer other than ambient air and (b) rigid backing on the left. The plate flies into ambient air on its right. A specific example for the case of rigid backing in Fig. 6 shows the time evolution of the kinetic energy/area of the plate until the point that it attains its maximum velocity. In this example, almost 80% of the initial excess energy (11) in the compressed layer ΔE_0 is transferred to the plate. The figure also shows the evolution of the excess energy in the air to the left and right of the plate ΔE, defined as the sum of the kinetic energy and the excess internal energy in Eq. (12). The maximum velocity is attained after the plate has plowed into ambient air on its backside creating a pressure wave to the right of the plate.

It is no surprise that the role of the backing is enormous, as seen in Fig. 7. In this figure, the maximum kinetic energy/area transferred to the plate KE is normalized by the initial excess energy in the compressed layer ΔE_0 and plotted against m_p/m_0. As in Sec. 2.3, $m_0=h_{\text{atm}}\rho_{\text{atm}}=h\rho_0$ is the mass/area of the air in the compressed layer. The only other dimensionless parameter in this problem (other than γ and the viscosity coefficients) is $p_0/p_{\text{atm}}=(h_{\text{atm}}/h)^{\gamma}$. When the compressed layer has rigid backing, the plate acquires a significant fraction of the energy of the compressed layer, depending in detail on m_p/m_0 and p_0/p_{atm} as plotted in Fig. 7(*b*). With backing, highly compressed initial layers $(p_0/p_{\text{atm}}>100)$ acting on relatively massive plates $(m_p/m_0>10)$ transmit 80% or more of their energy to the plate. The maximum momentum/area transmitted to the plate can be obtained from $I=\sqrt{2m_p\text{KE}}$. By contrast, a plate launched by a compressed layer with no backing acquires a small fraction of ΔE_0 (Fig. 7(*a*)).

4.2 Finite Standoff *d* With Rigid Backing. The effect of a finite standoff distance d between the plate and the compressed layer is now considered, as depicted in Fig. 8. The compressed air layer has rigid backing. At $t=0$, ambient air exists between the compressed layer and the plate and also to the right of the plate. The normalized maximum kinetic energy acquired by the plate $\text{KE}/\Delta E_0$ is computed as a function of the standoff distance. In addition to the two dimensionless parameters introduced for the case of zero standoff p_0/p_{atm} and m_p/m_0, one new dimensionless standoff parameter comes into play. One possibility is d/h_{atm} and another is $p_{\text{atm}}d/\Delta E_0$; these parameters can be expressed in terms of one another using the other two dimensionless parameters. The choice d/h_{atm} is preferred because h_{atm} reflects the distance over which the highest pressures in the compressed layer will still persist as it expands. The results for one set of parameters p_0/p_{atm}

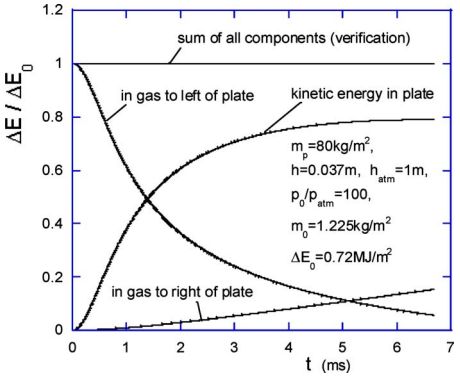

Fig. 6 An example for the case of the compressed layer with rigid backing and a plate with zero standoff distance. The evolution of the several components of the energy of the system with time is plotted until the time when the plate acquires its maximum velocity. The energy/area ΔE in the air to the left and right of the plate is the sum of the kinetic energy and the excess internal energy as defined in Eq. (12). As noted from the top curve, the numerical method conserves energy to a high degree of accuracy. In this example, value for m_p is equivalent to a 1 cm thick steel plate; the maximum velocity attained by the plate is 120 m/s.

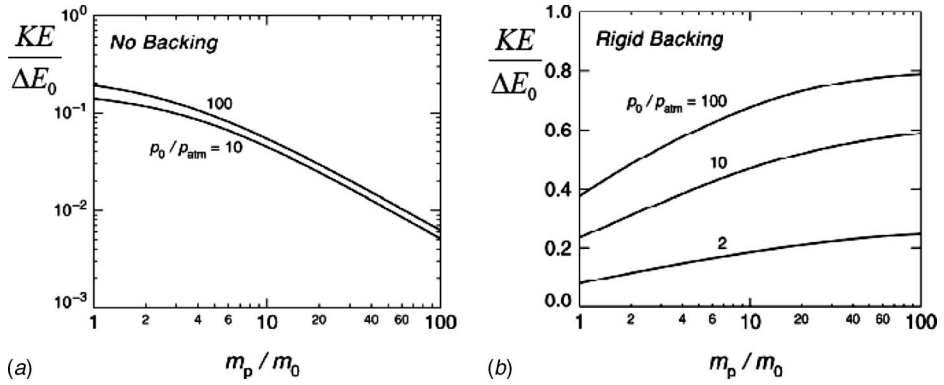

Fig. 7 Ratio of the maximum kinetic energy/area transmitted to plate to the initial excess energy/area in the compressed layer for the case with no standoff between the plate and the layer. (*a*) No backing to the compressed layer. (*b*) Rigid backing to the compressed layer.

$=100$ and $m_p/m_0=100$ are plotted as a function d/h_{atm} in Fig. 9. The exceptionally strong effect of the standoff distance is evident, as will now be discussed.

The kinetic energy transferred to the plate drops dramatically as the standoff distance increases. For the example given in the caption of Fig. 9 with a specific choice of dimensions, the kinetic energy transferred to the plate is already reduced substantially at the standoff $d \cong h_{\text{atm}}=0.33$ m. The limit for large standoff labeled in Fig. 9 is readily understood using the result in Sec. 2.3 for the momentum of a wave generated by the release of the compressed air layer in a semi-infinite region in conjunction with the fluid-structure interaction results in Fig. 4. With reference to Fig. 3(*b*), note that the momentum/area of the rightward moving wave generated by a compressed layer with $p_0/p_{\text{atm}}=100$ is $I \cong 1.05\sqrt{\Delta E_0 m_0}$, assuming the wave has been propagated sufficiently far to be fully developed with a well defined momentum. Assuming this is the case, identify I with the momentum/area I_0 of the wave hitting the plate and ΔE_0 as the wave energy/area. By Eq. (16), $\beta \cong 0.55(m_0/m_p)=0.0055$ and, thus, from Fig. 4, the momentum/area transferred to the plate is nearly $2I_0 \cong 2.1\sqrt{\Delta E_0 m_0}$. Then, because the kinetic energy/area of the plate is

$$\text{KE} = (2I_0)^2/(2m_p) \cong 2.2\Delta E_0(m_0/m_p)$$

the large standoff limit is

$$\frac{\text{KE}}{\Delta E_0} \cong 2.2\frac{m_0}{m_p} \tag{18}$$

For the set of parameters in Fig. 9 this limit is 0.022. The example in Fig. 9 is representative for any relatively massive plate (i.e., $m_p/m_0>10$) in any intense air blast.

The standoff effect illustrated in Fig. 9 is one-dimensional. It is quite distinct from the more easily understood effect of standoff in two and three dimensions wherein the blast wave intensity, as measured by the momentum/area and/or energy/area, diminishes inversely as a function of distance as the wave propagates away from the source. In the one-dimensional situation considered here with backing and no standoff, a large fraction of the air layer energy is converted directly into the kinetic energy of the plate as the layer expands against the plate (c.f., Fig. 7(*b*)). At the other extreme, for large standoff, the energy in the compressed air layer is first converted into the energy of the propagating wave. When this wave hits the plate, a very small fraction of the wave energy is transferred to the plate because the wave bounces off the plate retaining much of its energy. In other words, with sufficient standoff (e.g., $d/h_{\text{atm}}>1$) for intense waves ($p_0/p_{\text{atm}}>10$) and relatively massive plates ($m_p/m_0>10$), most of the energy of the initial compressed layer remains trapped between the wall and the plate in the form of kinetic and internal energies of the air with waves reverberating back and forth between the wall and the plate.

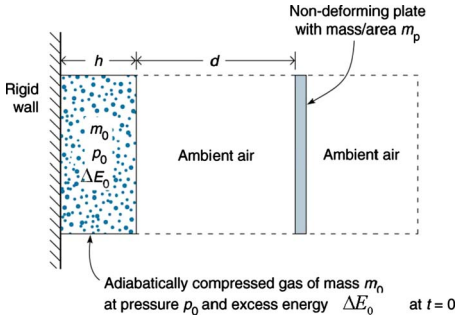

Fig. 8 Configuration for simulations of energy transferred to plate with standoff *d*. The compressed air layer has rigid backing.

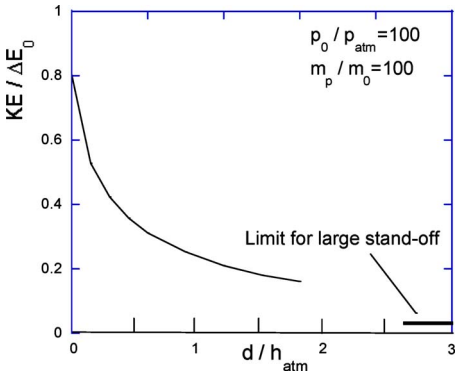

Fig. 9 The maximum kinetic energy/area transmitted to plate as a function of the standoff distance between the plate and the compressed air layer plotted for a specific set of dimensionless parameters. For reference, a set of dimensional parameters that corresponds to these results is: $h_{\text{atm}}=0.33$ m, $h=0.012$ m, $\Delta E_0=0.24$ MJ/m^2, $m_p=40$ kg/m^2, $m_0=0.4$ kg/m^2 and $p_0=10.5$ MPa. The limit for large standoff is discussed in the text.

5 Concluding Remarks

The study focused on one-dimensional waves in air modeled as an ideal gas. The main findings are as follows.

(a) For intense waves in air initiated by the sudden release of an adiabatically compressed layer, a relatively simple re-

lation exists between the energy in the compressed layer and the momentum of the ensuing wave as presented in Fig. 3.

(b) A massive plate struck by an isolated wave acquires twice the momentum of the incident wave. It remains to establish this result theoretically—it has been verified to a high degree of numerical accuracy in this paper.

(c) A presentation is given of fluid-interaction curves for the fraction of the momentum transferred to a freestanding plate in intense air blasts using invariants of the impacting wave (Fig. 4). While more comprehensive results have been presented by KNR [3] using other variables to describe the incident wave, the results given here provide additional insights to the interaction and have certain advantages stemming from the invariance of the parameters.

(d) The enormous effect of backing to the compressed layer on the energy transmitted to a plate in direct contact with the layer is quantified.

(e) Standoff between the plate and the compressed layer also has a very large effect in a one-dimensional setting. If the standoff is sufficiently large such that a well developed wave forms prior to impacting the plate, relatively little of the initial energy in the compressed layer is transmitted to the plate.

Acknowledgment

This work was supported in part by the ONR through Grant No. N00014-07-1-0764 and in part by the School of Engineering and Applied Sciences, Harvard University.

References

[1] Taylor, G. I., 1963, "The Pressure and Impulse of Submarine Explosion Waves on Plates," *The Scientific Papers of Sir Geoffrey Ingram Taylor*, G. K. Batchelor, ed., Cambridge University Press, Cambridge, UK, Vol. 3, pp. 287–303.
[2] Cole, R. H., 1948, *Underwater Explosions*, Dover, New York.
[3] Kambouchev, N., Noels, L., and Radovitzky, R., 2006, "Nonlinear Compressibility Effects in Fluid-Structure Interaction and Their Implications on the Air-Blast Loading of Structures," J. Appl. Phys., **100**, p. 063519.
[4] Kambouchev, N., Noels, L., and Radovitzky, R., 2007, "Fluid-Structure Interaction Effects in the Dynamic Response of Free-Standing Plates to Uniform Shock Loadings," ASME J. Appl. Mech., **74**, pp. 1042–1045.
[5] Liepmann, H. W., and Roshko, A., 1957, *Elements of Gas Dynamics*, Wiley, New York.
[6] von Neumann, J., and Richtmyer, R., 1950, "A Method for the Numerical Computation of Hydrodynamic Shocks," J. Appl. Phys., **21**, pp. 232–237.
[7] Drumheller, D. S., 1998, *Introduction to Wave Propagation in Nonlinear Fluids and Solids*, Cambridge University Press, Cambridge, UK.
[8] Sedov, L. I., 1993, *Similarity and Dimensional Methods in Mechanics*, 10th ed., CRC, Boca Rotan, FL.
[9] von Neumann, J., 1943, "The Point Source Solution," *Collected Works*, Vol. 6, Pergamon, New York, pp. 219–237.
[10] Kambouchev, N., 2007, "Analysis of Blast Mitigation Strategies Exploiting Fluid-Structure Interaction," Ph.D. thesis, Department of Aeronautics and Astronautics, Massachusetts Institute of Technology, Cambridge, MA.